J. Fluid Mech. (2002), *vol.* 455, *pp.* 83–101. © 2002 Cambridge University Press
DOI: 10.1017/S0022112001007364 Printed in the United Kingdom

Vortex merger in rotating stratified flows

By DAVID G. DRITSCHEL
Mathematical Institute, University of St Andrews, North Haugh, St Andrews KY16 9SS, Scotland

(Received 1 September 2000 and in revised form 31 August 2001)

This paper describes the interaction of symmetric vortices in a three-dimensional quasi-geostrophic fluid. The initial vortices are taken to be uniform-potential-vorticity ellipsoids, of height $2h$ and width $2R$, and with centres at $(\pm d/2, 0, 0)$, embedded within a background flow having constant background rotational and buoyancy frequencies, $f/2$ and N respectively. This problem was previously studied by von Hardenburg *et al.* (2000), who determined the dimensionless critical merger distance d/R as a function of the height-to-width aspect ratio h/R (scaled by f/N). Their study, however, was limited to small to moderate values of h/R, as it was anticipated that merger at large h/R would reduce to that for two columnar two-dimensional vortices, i.e. $d/R \approx 3.31$. Here, it is shown that no such two-dimensional limit exists; merger is found to occur at any aspect ratio, with $d \sim h$ for $h/R \gg 1$.

New results are also found for small to moderate values of h/R. In particular, our numerical simulations reveal that asymmetric merger is predominant, despite the initial conditions, if one includes a small amount of random noise. For small to moderate h/R, decreasing the initial separation distance d first results in a weak exchange of material, with one vortex growing at the expense of the other. As d decreases further, this exchange increases and leads to two dominant but strongly asymmetric vortices. Finally, for yet smaller d, rapid merger into a single dominant vortex occurs – in effect the initial vortices exchange nearly all of their material with one another in a nearly symmetrical fashion.

1. Introduction

Vortices play a central role in the evolution of high-Reynolds-number flows. Regions of intense swirling motions are highly energetic and generally move as material volumes, making them conspicuous features. In stably stratified, rotating flows, such as the Earth's atmosphere and oceans, these vortices are readily identified by their anomalous 'potential vorticity' (PV) $q(x, y, z, t)$, a scalar quantity which is materially conserved in the absence of diabatic forcing or dissipation. In the real atmosphere and oceans, the PV is sufficiently well conserved in many regions to merit special attention. The three-dimensional distribution of this dynamical tracer to a great extent determines the three-dimensional flow field (cf. Hoskins, McIntyre & Robertson 1985). In turn, the flow field modifies q, strictly speaking 'rearranges' it, giving rise to a new flow field, and so on. When q is perfectly conserved, and when q completely determines the flow field (as in 'balanced', gravity-wave-free approximations of the full governing equations), then a material Lagrangian description of the fluid motion in terms of coherent regions of q, 'vortices', can be used to great advantage. The flow evolution is then controlled by the motion of the vortices, in particular their interactions with each other.

Many studies have focused on the idealized interaction of vortices, the merging

https://doi.org/10.1017/S0022112001007364 Published online by Cambridge University Press

of two vortices in particular, and almost all of these studies have considered a two-dimensional fluid (independent of one spatial coordinate, say of z). A two-dimensional fluid may be regarded as a limiting case of a three-dimensional rotating stably stratified fluid between narrowly separated rigid (stress-free) horizontal boundaries. In this case, there is no scope for vertical variations, and the flow remains two-dimensional if initially so.† Originally, however, a two-dimensional fluid was regarded as an approximation to a three-dimensional non-rotating unstratified fluid, in aerodynamics (see e.g. Saffman 1992). In any case, one of the first problems examined was the merger of two identical 'symmetric' vortices by Christiansen & Zabusky (1973). They employed a particle-in-cell numerical algorithm to follow clouds of point vortices initially distributed uniformly over two circular disks of radius R and separated by a distance d centre-to-centre. Their simulations indicated that, for $d \lesssim 3.4R$, the two vortices (or vortex clouds) coalesce or 'merge' into one, along with some filamentary remnants, while for $d \gtrsim 3.4R$, the vortices interact elastically, with no evidence of merging, at least over the period of time simulated. More recently, the critical merger distance was pinned down to $d = d_c \approx 3.31R$ by Waugh (1992) using accurate contour dynamics simulations. (See Waugh 1992 for a review of other works on this problem.)

Several studies have generalized this two-dimensional problem to consider the effect of vertical structure on vortex merger. All of these studies have used the simplest balanced system applicable to rotating, stably stratified flows, namely the 'quasi-geostrophic' (QG) one (described in § 2). Of most direct relevance is the work of Verron, Hopfinger & McWilliams (1990), who determined the conditions for vortex merger in a two-layer QG fluid. These conditions depend on several parameters: the layer depth ratio, the ratio of the potential vorticity (PV) in each layer, as well as the distance between vortex centres. But the utility of these results for a three-dimensional, many-layer flow is not clear. Do new phenomena occur? Is the detailed vertical structure important?

Two recent studies have examined vortex interactions in three-dimensional QG flows. Dritschel & de la Torre Juárez (1996, hereafter DTJ), considered two initially columnar (two-dimensional) vortices in mutual equilibrium (cf. Dritschel 1995) within a domain of depth H. They showed that, for sufficiently large H/R, where R is the mean vortex radius, arbitrarily small vertical disturbances induce the vortices to break down three-dimensionally, eventually resulting in vortex merger at either the upper or lower surface of the domain and the formation of two roughly hemispherical domes of PV at the opposite surface. At sufficiently small H/R, the vortices merge just as in a two-dimensional fluid – then, three-dimensional disturbances do not amplify significantly. These results were shown to be a consequence of a three-dimensional instability that occurs when $H/R \gtrsim 6f/N$, where f and N are the frequencies associated with the background rotation and buoyancy.

More recently, von Hardenburg *et al.* (2000, hereafter HX), studied the merging of two ellipsoidal distributions of PV in a triply periodic domain (approximating an unbounded domain). Each ellipsoid was given a common half-height h, a radius R, and a cosine-shaped profile of PV increasing inwards across ellipsoidal surfaces of fixed aspect ratio h/R (several additional simulations were performed using uniform-PV profiles that indicate only a weak sensitivity to the PV profile). The two ellipsoids were located at the same vertical level and their centres were separated horizontally

† This is strictly true only for horizontal scales $L \gg NH/f$, where H is the depth of the fluid, and N and f are the buoyancy and rotational frequencies – see Dritschel, de la Torre Juárez & Ambaum (1999).

https://doi.org/10.1017/S0022112001007364 Published online by Cambridge University Press

by a distance d. By varying d in a series of numerical simulations, HX estimated the dimensionless critical merger distance d_c/R as a function of h/R, over the range $0.16f/N \leqslant h/R \leqslant 3.5f/N$.

For $h/R \ll f/N$, they find that d_c/R tends to a constant around 2.2, i.e. the vortices must be nearly touching initially for merger to occur. On the other hand, their results for the largest values of h/R examined indicate $d_c/R \propto h/R$. They did not consider it necessary however to examine still larger values of h/R, but instead relied upon earlier results for the merger of vortices in a two-layer QG fluid (Verron *et al.* 1990) which indicated that d_c eventually asymptotes the two-dimensional result, $d_c = 3.3R$, as $h/R \to \infty$, after a small overshoot. By contrast, the results of DTJ, for a many-layer fluid, show a clear three-dimensionalization at sufficiently large vortex aspect ratios, with vortex merger near the top and bottom boundaries and locations in between, depending on the initial aspect ratio (see also Dritschel & Macaskill 2000).

DTJ did not consider ellipsoidal vortices but columnar ones; moreover, they did not consider periodic vertical boundaries. But nor did Verron *et al.* (1990). What then is to be expected at larger aspect ratios? To answer this question, a large number of simulations of the interaction of two identical uniform-PV ellipsoids have been carried out which cover a wide range of aspect ratios, up to $h/R = 20f/N$. Vortex merger has been found to occur also at these large aspect ratios and, moreover, d_c/R continues to increase approximately linearly with h/R. These results are described in § 3, after a description of the physical system, problem setup and numerical methods in § 2. The relation of these numerical results to the linear instability of vortex columns described by DTJ is discussed in § 4. The conclusions are given in § 5.

2. Problem formulation

As in HX, we consider here the simplest fluid dynamical system embodying the two basic ingredients of rotation and stable stratification. This *quasi-geostrophic* (QG) system is obtained from the full 'primitive' equations by an asymptotic expansion in three small parameters: (i) the height-width aspect ratio H/L of characteristic motions (constrained to be small due to the shallow geometry); (ii) the Rossby number R_o or ratio of the normal component of the relative vorticity ζ to the normal component of the background vorticity $f = 2\Omega \sin\phi$, where Ω is the planetary rotation rate and ϕ is the latitude; and (iii) the Froude number F_r or the ratio of relative (horizontal) fluid speed U to the wave speed associated with stratification $c = NH$, where N is the buoyancy frequency. (For the ocean, $N = \sqrt{-g\rho^{-1}\partial\rho/\partial z}$ where ρ is the density and g is the acceleration due to gravity.) Note that in the atmosphere, $f/N \sim 10^{-2}$ while in the oceans, $f/N \sim 10^{-1}$. Quasi-geostrophy is obtained assuming $H/L \ll 1$ and $F_r^2 \ll R_o \ll 1$ (see for instance Stegner & Zeitlin 1995).

Here, as in HX, we take f and N to be constant and consider a *Boussinesq* fluid in which the density varies little across the depth of the domain considered. Then it is appropriate to rescale the vertical coordinate z by f/N, for then the governing equations may be expressed in a parameter-free way as

$$\frac{\partial q}{\partial t} + \boldsymbol{u}\cdot\nabla q \equiv \frac{\mathrm{D}q}{\mathrm{D}t} = 0, \tag{1a}$$

$$\nabla^2\psi = q, \tag{1b}$$

$$u = -\frac{\partial\psi}{\partial y}, \quad v = \frac{\partial\psi}{\partial x}, \tag{1c,d}$$

https://doi.org/10.1017/S0022112001007364 Published online by Cambridge University Press

where $\boldsymbol{u}$ is the horizontal geostrophic velocity, ψ is the streamfunction, and ∇^2 is the three-dimensional Laplacian. Note that, to this order of approximation in the governing equations, $O(F_r)$, there is no vertical motion: $w = 0$. The advection of PV in (1a) is purely horizontal. If we drop $\partial^2\psi/\partial z^2$ from (1b), we recover the purely two-dimensional system.

For the numerical simulation of the flow evolution, HX used a finite-difference multi-grid method and employed periodic boundaries in both vertical and horizontal directions. Here, we also employ periodic boundaries but use a different numerical method, the 'contour-advective semi-Lagrangian' (CASL) algorithm (Dritschel & Ambaum 1997). The CASL algorithm combines contour surgery (CS, Dritschel 1989) with a standard pseudo-spectral (PS) method. In this way, it benefits from the accuracy of CS (which follows PV contours in a Lagrangian way) and the efficiency of PS (which can rapidly compute the velocity field by Fourier transforms). Moreover, Lagrangian advection lifts the CFL stability constraint, and a contour representation of the PV allows one to represent fine-scale structure well below the scales accessible to conventional numerical methods. The upshot is that, for a given accuracy, the CASL algorithm is typically hundreds of times faster than either CS or PS in complex flow simulations (Dritschel, Polvani & Mohebalhojeh 1999).

A second numerical method, based purely on CS, is also employed (see Appendix A for the details of this method). This CS algorithm permits one to study the flow evolution in an unbounded domain, freeing one from the unwanted effects of periodicity, but simulations are costly. However, the effects of periodicity turn out to be significant for all but shallow vortices, despite using vortices that are small compared to the domain dimensions (and smaller than those simulated by HX). For this reason, nearly all of the simulations were conducted using CS except for the small aspect ratio cases $h/R < 0.5$, which were not found to be sensitive to the domain periodicity (details are given below).

The initial flow consists of two uniform-PV ellipsoids, centred at $\boldsymbol{x} = (\pm d/2, 0, 0)$, having a circular horizontal cross-section, maximum radius R, and half-height h. The bounding surface of each vortex is given by

$$\frac{(x \mp d/2)^2 + y^2}{R^2} + \frac{z^2}{h^2} = 1$$

and within each vortex, the potential vorticity $q = Q$, a constant, while outside $q = 0$. (In the periodic case, the fact that the domain integral of $\nabla^2\psi$ must vanish implies that there is a small background value of q distributed uniformly throughout the domain.) We take $Q = 4\pi$ without loss of generality. A two-dimensional circular vortex with this value of q would rotate exactly once in one unit of time.

The choice of a uniform PV distribution is primarily one of convenience and maximum simplicity. While real vortices are likely to have more complex, non-uniform distributions, interactions with other vortices tend to steepen edge PV gradients by stripping away low-lying peripheral PV (see Yao, Dritschel & Zabusky 1995 for the two-dimensional case). Even weak shear and strain associated with distant vortex interactions can leave a vortex with a practically discontinuous jump in PV at its edge (see Caillol, Legras & Dritschel 2001 and references therein, again for the two-dimensional case). This together with the close similarities between the two-dimensional and three-dimensional fluid models implies that, when diffusion is weak, typical vortices have for all practical purposes *compact* PV distributions. Such distributions are quite well approximated by uniform PV.

For the CASL simulations, the domain has dimensions $L \times L \times D$ with $L = 2\pi$

https://doi.org/10.1017/S0022112001007364 Published online by Cambridge University Press

(without loss of generality) and the depth D chosen as follows. Given the parameters h/R and d/R, first the radius is computed from $R = 2/(2 + d/R)$, which means that the outermost edges of the vortices at the mid-plane $z = 0$ touch $x = \pm 1$. This is done to keep the periodic boundaries far from the vortices. Then, the height of the domain is chosen from $H = 2\pi \max(R, h)$, where $h = (h/R)R$. This ensures that the vertical extent of the vortices is small compared with that of the domain. The numerical resolution is chosen according to the conditions that each vortex spans 40 layers vertically and at least 10 grid points horizontally at mid-section (the actual horizontal grid resolution is chosen to be a convenient multiple of 2, 3 and 5 to permit efficient FFTs). Note that in the CASL algorithm, the PV is resolved to one tenth of the basic grid scale and that some of this sub-grid-scale PV actually contributes to the velocity field (a twice finer grid is used to convert the PV contours to gridded values during the velocity calculation; see Dritschel & Ambaum 1997 for details of this and other numerical parameters, as well as accuracy tests; see also Dritschel *et al.* 1999 for a recent inter-algorithm comparison).

For the CS simulations, 40 layers are used to represent the vertical structure of each vortex, except in a few higher resolution examples noted below. Tests indicate no sensitivity of the critical merger distance to increases in vertical resolution, at least to the digits reported below. Contours are resolved with a maximum dimensionless point separation of $\mu = 0.15$ and regularized at the surgical scale of $\delta = \frac{1}{4}\mu^2\ell = 0.01125R$, where $\ell = 2R$ is a length characterizing the PV distribution. The time step in both the CS and CASL simulations is $\Delta t = 0.025$, the recommended value for high accuracy.

As stated above, the CS simulations allow for a check on the effects of periodicity (horizontal and vertical) within the CASL simulations. One would expect that these periodic effects diminish with decreasing vortex size, keeping the domain size fixed, but one cannot reduce the vortex size indefinitely in CASL or in any periodic code (like that used by HX) due to the growing cost necessary to resolve each vortex adequately. In the CASL simulations, the vortices are confined to the inner 3% or less of the domain volume, yet the effects of periodicity are still evident, particularly on the sensitive estimate of the critical merger distance, and especially for $h/R \gg 1$. For example, when $h/R = 1$, the critical merger distance is 4% smaller in CASL than it is in CS, while when $h/R = 0.5$, it is 2% smaller. Notably, HX used a much less stringent criterion for choosing the vortex sizes; each vortex had a diameter of $\frac{1}{2}\pi$ regardless of their separation d, and no vertical extension of the domain beyond 2π was made for their large aspect ratio cases. For those cases, both the horizontal and the vertical extent of the initial conditions exceeded half the domain dimensions. As a result, the quantitative estimates of the critical merger distance made by HX may not be reliable.

3. Results

The simulation results are broken down into three regimes, depending on the initial aspect ratio h/R.

3.1. *The regime* $h/R \leqslant 1$

These shallow, lens-like vortices must be close together for merging, as found in HX, though they need not be in near contact. For example, when $h/R = 0.2$, the vortices merge if $d/R \leqslant 2.5 \approx d_c/R$; this critical case (for $d/R = 2.5$) is shown in figure 1. For all cases in this regime, vortices placed just within the critical merger distance first form a bridge with one another, creating a dumbbell-shaped vortex which rotates

https://doi.org/10.1017/S0022112001007364 Published online by Cambridge University Press

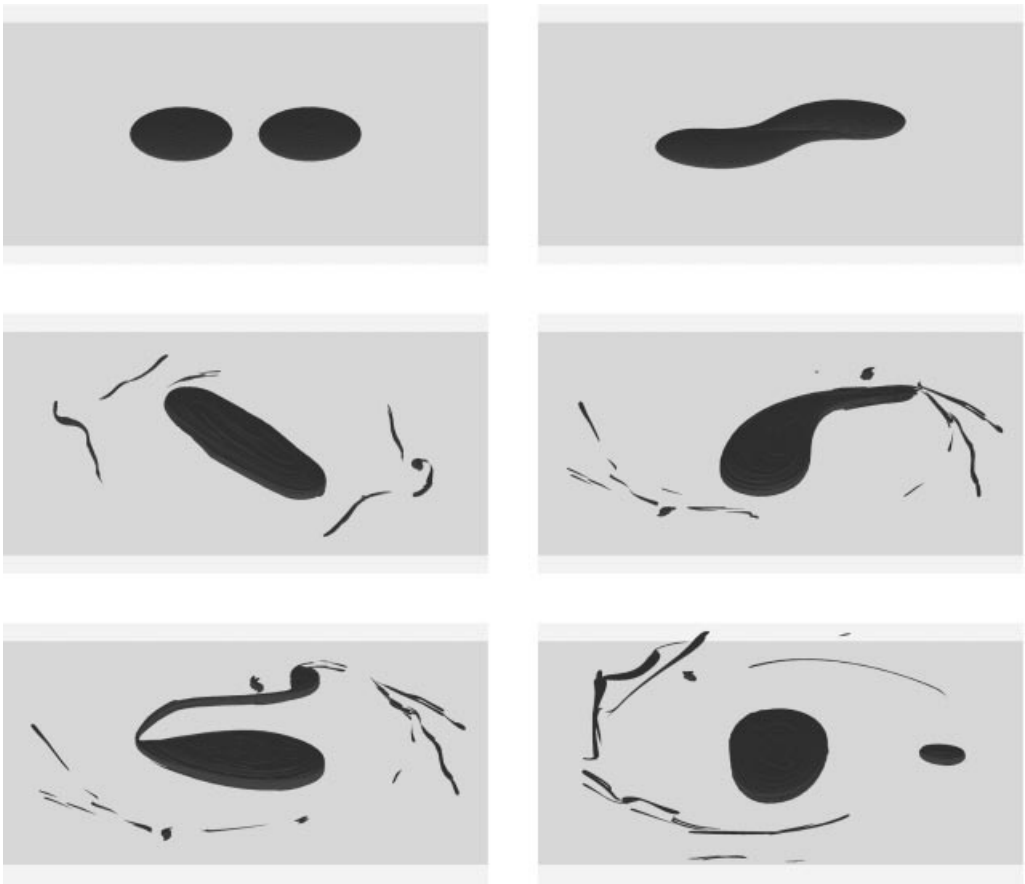


FIGURE 1. Evolution sequence for two lens-like vortices with $h/R = 0.2$ and $d/R = 2.5$, as computed using the CASL algorithm (using the basic grid resolution $72 \times 72 \times 628$). Time advances to the right and downwards, with times $t = 0, 3, 26, 48, 53$ and 137 displayed. The vortices are viewed from an infinite vantage point (orthographic projection) at an angle of 30° from the vertical and in the plane $x = 0$. Only the inner part of the domain $|x| < 2\pi/3$, $|y| < 2\pi/3$, $|z| < h$ is shown. The front and back vertical faces of the domain are rendered in a lighter shade of gray. The floor of the domain which is not obscured by the front face is rendered a slightly darker shade.

steadily (evidently as a near-equilibrium structure) for a long period of time before eventually destabilizing. Then, two unequal vortices form, something not seen in the analogous simulations conducted by HX. In the case shown in figure 1, the secondary vortex is very small, just 6% of the volume of the primary vortex, but when d/R is increased, the relative volume of this secondary vortex is also increased. Figure 2, for example, shows how the volume ratio of the two largest vortices varies with d/R when $h/R = 0.5$. This volume ratio appears to be a monotonic function of d/R for all aspect ratios.

This asymmetric evolution was not seen in the simulations of HX because they enforced two-fold symmetry. The simulations here do not enforce this symmetry (arguably Nature does not either), and they reveal a radically different view of 'vortex merger'. Indeed, 'merger' is clearly an inadequate description of what actually occurs here. A range of interactions is found, depending continuously on d/R. For definiteness, we may call interactions in which the final secondary vortex or

https://doi.org/10.1017/S0022112001007364 Published online by Cambridge University Press

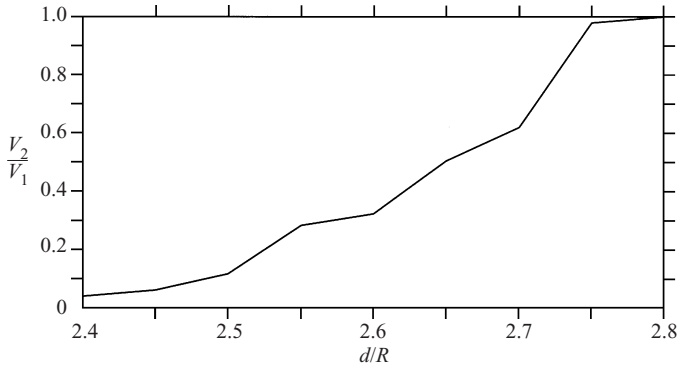


FIGURE 2. The ratio of the final volumes of the next-to-largest and largest vortices as a function of d/R, for vortices of initial height-to-width aspect ratio $h/R = 0.5$.

vortices constitute less that 10%, say, of the volume of the primary vortex 'complete merger', following the nomenclature introduced earlier for two-dimensional vortex interactions (Dritschel & Waugh 1992). A difference from the two-dimensional case is that here secondary vortices are almost always produced because of the weaker shear surrounding three-dimensional vortices (cf. Waugh & Dritschel 1991), so it is virtually impossible to have complete merger in the original sense. All other interactions which lead to a change in volume of the primary vortex are called 'partial merger', except when the volume of the secondary vortex differs by less than 10% of the primary vortex. We will call such interactions 'weak exchange', as only a small amount of material is exchanged between the vortices before they reseparate. These three forms of interaction are present up to and including $h/R = 1.75$.

3.2. *The regime* $1 < h/R \leqslant 3$

In this regime, vortex interactions are characterized by a substantial production of filamentary debris and small-scale vortices (from the roll-up of the debris ejected furthest from the main product vortex). Figure 3 shows an example of complete merger at the lower end of this regime ($h/R = 1.5$, $d/R = 2.9$, volume of the secondary vortices = 8.8% that of the primary vortex at $t = 53$). Here, after the initial extended merger of the two vortices, one side of the compound vortex shears vertically, with the middle part (in z) being pulled into the main vortex and its outer tips expelled into thick filaments spiralling around the consolidating vortex. The tips of these two filaments eventually roll up into significant vortices, and many smaller-scale vortices are generated in a similar manner. The filaments thin and disperse in the straining/shearing environment surrounding the vortices, and at late times only three significant vortices survive. Towards the upper end of this regime, a new phenomenon can be seen – figure 4 shows the case $h/R = 2.5$, $d/R = 3.4$, an example of partial merger (volume of the secondary vortices = 11.7% that of the primary vortex at $t = 47.5$). As in the previous case, many vortex roll-ups occur, but here the main vortex tilts over and precesses about the z-axis, evidently a sign that the vertically orientated state is unstable. This tilt develops over a short period of time, and afterwards it displays a periodic behaviour – see figure 5. This asymmetric behaviour was not found in the simulations conducted by HX, again because of the two-fold symmetry enforced by their numerical method.

https://doi.org/10.1017/S0022112001007364 Published online by Cambridge University Press

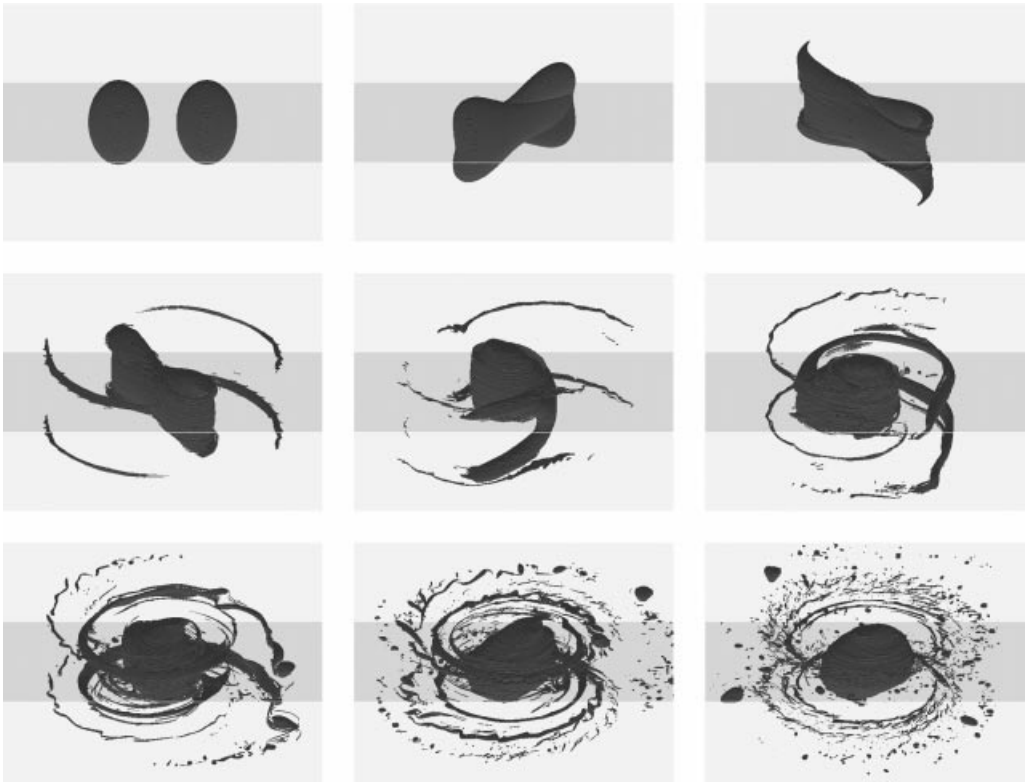


FIGURE 3. Evolution sequence for the case $h/R = 1.5$, $d/R = 2.9$ (computed using the CS algorithm with 100 layers). Times $t = 0, 1.5, 4, 8, 12, 16, 20, 32$ and 53 are displayed. The computational domain is here unbounded, but the perspective and rendering in this and all subsequent figures of the flow evolution is the same as in figure 1.

3.3. *The regime* $h/R > 3$

For greater aspect ratios, beyond those considered by HX, merger is found to continue from greater initial separation distances, with $d \sim h$. In this regime, only partial merger (or no merger) is found. The result of partial merger is one dominant, erect vortex centred at the origin plus a great many smaller vortices encircling it, particularly above and below the dominant vortex. As h/R increases, the total relative volume of these smaller vortices increases, and for $h/R \gtrsim 5$, exceeds that of the dominant vortex (by as much as 1.96 times in the case $h/R = 20$, $d/R = 12.6$).

The flow evolution in all cases is qualitatively similar. At first, the vortices deform into a boomerang shape, with the mid-sections near $z = 0$ advancing faster azimuthally about the joint centre of the two vortices, the z-axis. This makes sense from the form of the flow field induced by one ellipsoid on another: the azimuthal velocity is strongest at $z = 0$ and weakest at the vortex extremities. The vortices then rotate counter-clockwise so that their mid-sections move radially inwards while their extremities move outwards. This motion is self-induced by the vortex deformation. The closer proximity of the vortex mid-sections implies an even stronger azimuthal propagation and bending, and in turn the inward motion of the vortex mid-sections through self-induced rotation. If this rotation works faster than the azimuthal bending, the vortex centres pass each other at too great a distance and begin the whole process in reverse, eventually returning the vortices to a near ellipsoidal form; this

https://doi.org/10.1017/S0022112001007364 Published online by Cambridge University Press

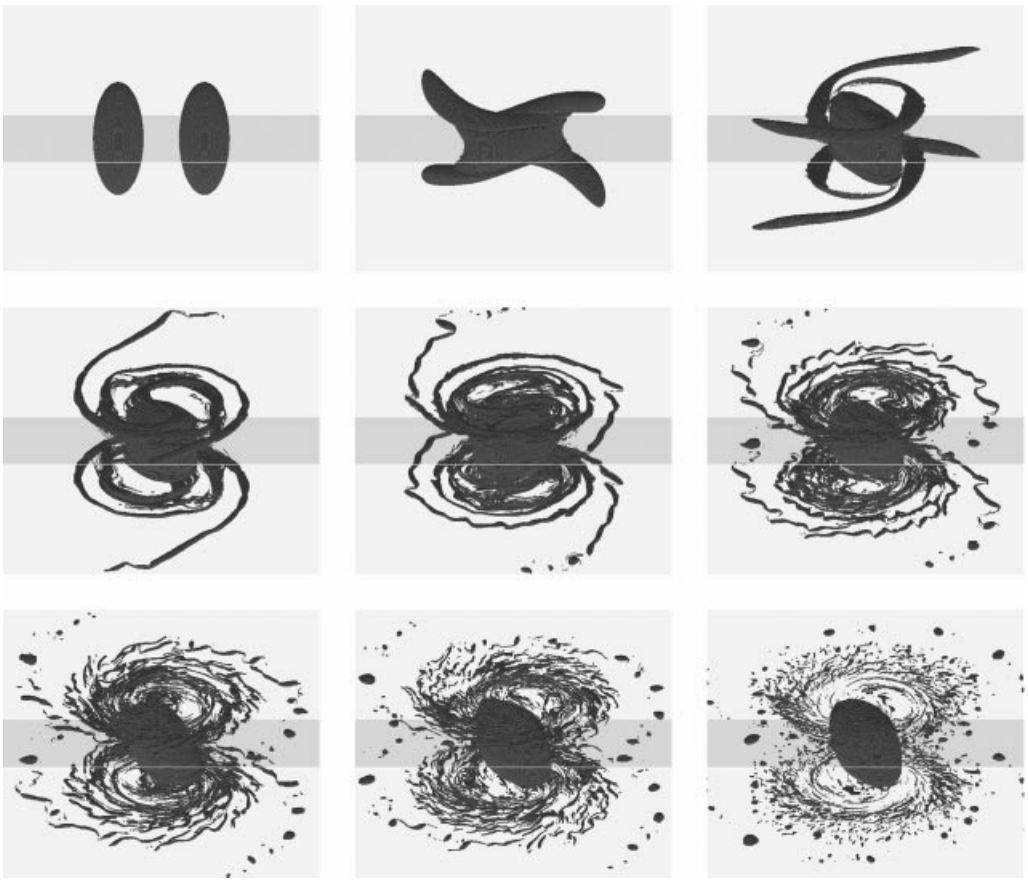


FIGURE 4. Evolution sequence for the case $h/R = 2.5$, $d/R = 3.4$ (computed using CS with 100 layers). Times $t = 0, 6, 9.5, 16, 21, 26, 29, 33$ and 46 are displayed.

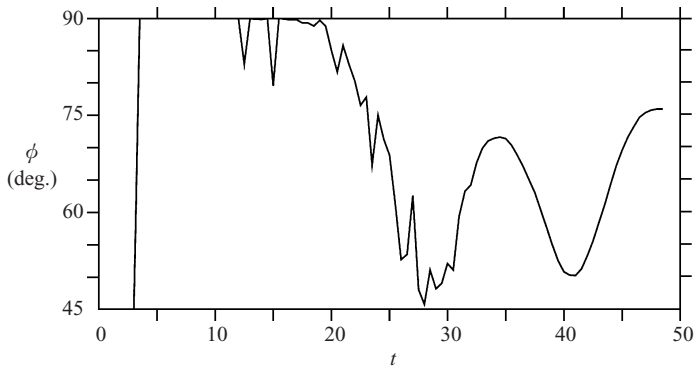


FIGURE 5. The angle ϕ between the major axis of the vortex and the vertical axis versus time for the case shown in figure 4. This angle is found by fitting the second-order spatial moments (the integrals of x^2, xy, xz, y^2, yz and z^2 over the largest contiguous vortex) to an arbitrarily orientated ellipsoid. When the two original vortices first merge, $\phi = 90°$ because the major axis then lies in the (x, y)-plane. The subsequent decrease of ϕ means that the major axis tilts out of the (x, y)-plane, here by between 15 and 45°.

https://doi.org/10.1017/S0022112001007364 Published online by Cambridge University Press

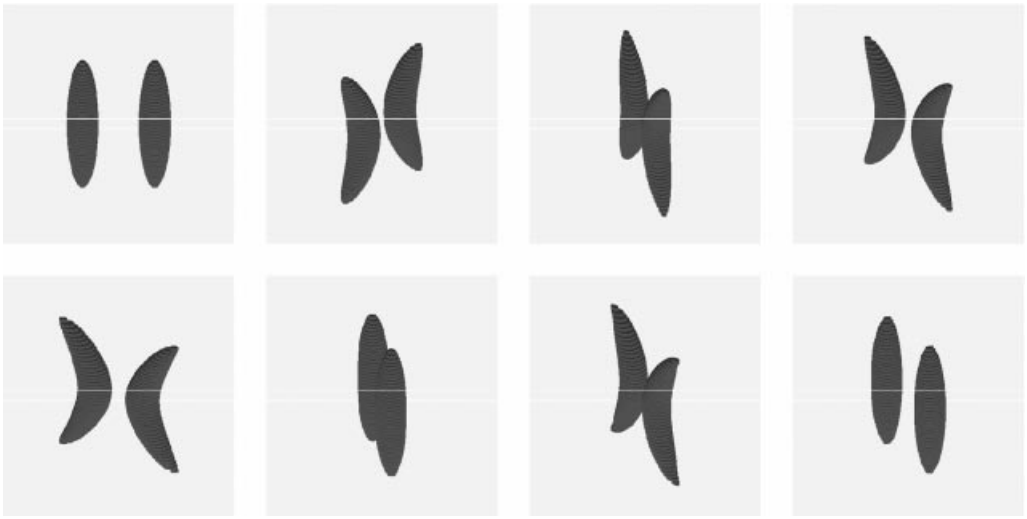


FIGURE 6. Evolution sequence for the case $h/R = 4.5$, $d/R = 4.5$ (computed using CS with 40 layers). Times $t = 0, 3, 6, 7, 8, 15, 25$ and 45 are displayed.

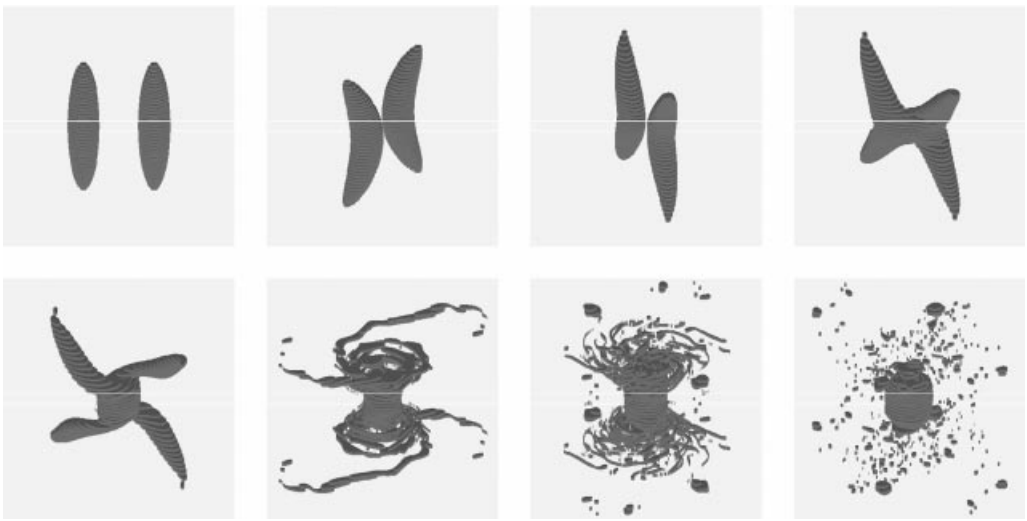


FIGURE 7. As in figure 6, but for $d/R = 4.4$. The same times are displayed except for the last (which is $t = 47$ here).

is shown in figure 6 for the case $h/R = 4.5$, $d/R = 4.5$. Reducing d/R to 4.4 results in merger – see figure 7. The mid-sections collide and form a moderately tall ellipsoidal vortex at late times. The extremities form a progressively tighter spiral which eventually destabilizes, forming a multitude of small-scale vortices and filamentary structures. This behaviour typifies all the large aspect ratio cases studied – see for example figure 8 for the case $h/R = 10$ and $d/R = 7.6 \approx d_c/R$.

3.4. *Critical merger distance*

Figure 9 summarizes the results of the approximately 100 simulations performed; in 9(a) the dimensionless critical merger distance d_c/R is plotted versus h/R, while in 9(b) an enlargement for $h/R \leqslant 3$ is plotted. First of all, this enlargement shows

https://doi.org/10.1017/S0022112001007364 Published online by Cambridge University Press

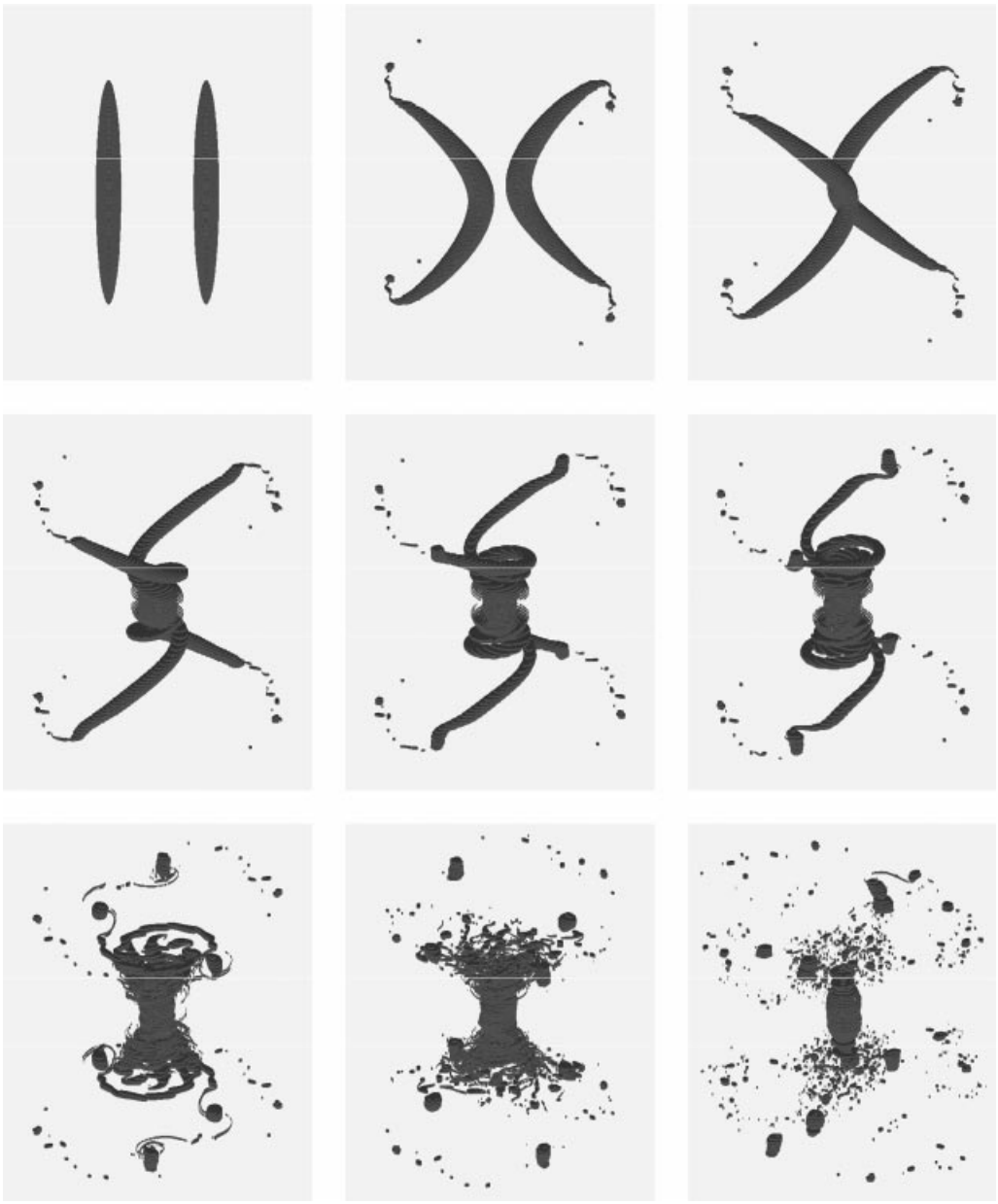


FIGURE 8. Evolution sequence for the case $h/R = 10$, $d = 7.6R \approx d_c$ (computed using CS with 100 layers). Times $t = 0, 25, 27, 29, 31, 33, 40, 50$ and 103.5 are displayed.

that the interaction between two vortices is more complex than was previously thought. The reason is that asymmetries rapidly develop if permitted initially – they evidently develop faster than symmetric disturbances, despite the near symmetry of the initial conditions, unless the vortices are initially close together, in which case complete merger occurs. In a complex flow, where vortices may be driven together by other vortices further afield, the interaction regimes first encountered would be weak exchange and partial merger, which suggests that these regimes may be more likely

https://doi.org/10.1017/S0022112001007364 Published online by Cambridge University Press

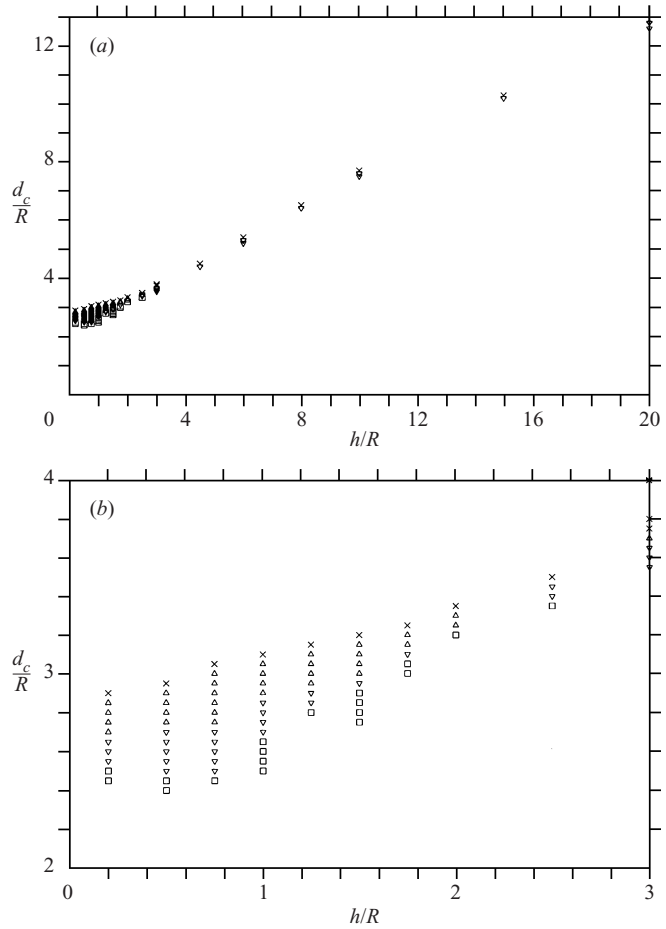


FIGURE 9. (*a*) Dimensionless critical merger distance d_c/R as a function of the initial vortex aspect ratio h/R. (*b*) Enlargement of (*a*) detailing the forms of interaction that occur for $h/R < 3$. Here CM = complete merger (indicated by squares), PM = partial merger (inverted triangles), WE = weak exchange (triangles), and EI = elastic interaction (crosses).

than complete merger. While it is certainly premature to draw general conclusions from the interaction of initially identical vortices, the preference for weak exchange and partial merger could have a crucial influence on the vortex size distribution in turbulence.

The other striking result here is the continued, evidently unabated growth of the critical merger distance with vortex height. This suggests that the two-layer results of Verron *et al.* (1990) are not applicable to tall vortices. Indeed, one can see that, from the boomerang shapes exhibited by the tall vortices here, at least three layers are needed to capture any semblance of the merger of tall vortices. This has been verified in simulations of the interaction of two vortex columns in two or more layers. For parameters which lead to the merger of tall columns in three or more layers, two-layer vortices do not exhibit merger; instead the upper and lower layers of each vortex drift apart and then re-align quasi-periodically. This illustrates a serious deficiency of the two-layer approximation to continuous stratification.

https://doi.org/10.1017/S0022112001007364 Published online by Cambridge University Press

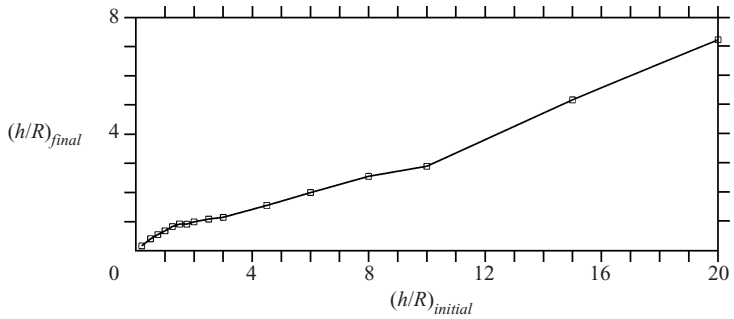


FIGURE 10. Comparison of the final and initial vortex height-to-width aspect ratios for vortices initially separated by the critical merger distance (this is the largest distance from which complete merger occurs, or, for tall vortices, from which partial merger occurs). The final value of h/R is determined from the second-order spatial moments, using $h = \sqrt{5M_{zz}/V}$ and $R = \sqrt{3V/4\pi h}$, where V is the vortex volume and M_{zz} is the integral of z^2 over the vortex.

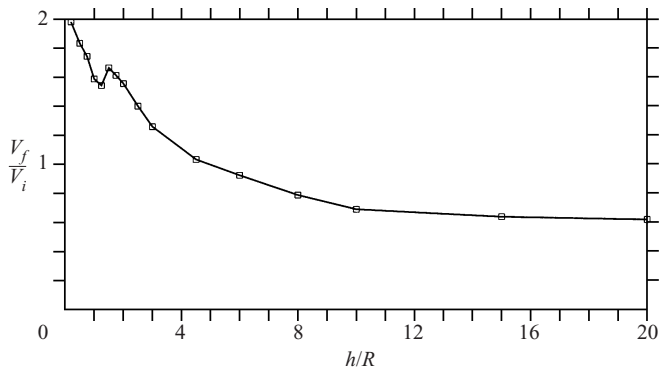


FIGURE 11. Volume of the largest product vortex divided by the volume of one of the original vortices as a function of the initial h/R and for vortices starting at the critical merger distance.

3.5. *Change in vortex aspect ratio*

HX also quantified the final aspect ratio of the merged vortices, and generally found values less than unity over the range of initial aspect ratios considered. They argued that their results supported an earlier analysis of vortex shapes in QG turbulence (McWilliams 1990). The results of the present study, for uniform-PV vortices, are shown in figure 10. A whole range of final aspect ratios are found, many exceeding unity. One can only say that merger results in flatter vortices. It is premature to argue that these results are relevant to QG turbulence however, since it is highly improbable that two interacting vortices in QG turbulence would be almost the same size and at almost the same vertical level for the present results to apply.

3.6. *Change in volume*

In two-dimensional flows, vortex merger is generally thought to result in a single, larger product vortex. Yet, this picture is misleading: vortex interactions are not typified by merger (Dritschel & Waugh 1992), and the largest product vortex is not always larger than the largest initial vortex, indeed it can be smaller (Dritschel 1995). Exactly what happens depends on the initial size ratio of the vortices and their separation. Here, for the three-dimensional case, we can only report what happens for highly symmetric initial conditions. For each initial aspect ratio h/R, figure 11

https://doi.org/10.1017/S0022112001007364 Published online by Cambridge University Press

shows the volume of the largest product vortex divided by the volume of one of the original vortices, for vortices initially separated by the critical merger distance d_c (as defined in the caption of figure 9). As $h/R \to 0$, the product vortex tends to double in size – there are very few filaments produced. This is also found in two-dimensional flows when the Green function has a short range (see Waugh 1992, who considered a Green function approximating the lens-like interactions considered here). As h/R increases, the volume ratio generally decreases, except for a region $1 \lesssim h/R \lesssim 2$. This may be associated with the onset of vortex tilting and precession (first observed at $h/R = 1.5$). The volume ratio remains greater than 1 until about $h/R = 4.5$, after which the largest product vortex is smaller than the original vortices. At large aspect ratios, many smaller vortices are produced, in addition to filaments. Interestingly, the volume ratio appears to asymptote 0.6 approximately (this is consistent with the nearly linear growth of the final vortex aspect ratio seen in figure 10).

4. The regime $h/R \gg 1$ and its relation to the tall-column instability

For a columnar, two-dimensional vortex vertically confined between two isothermal horizontal boundaries (at which $\partial\psi/\partial z = 0$), DTJ showed that an external, two-dimensional straining flow of the form

$$u_{\rm ext} = (\gamma + \Omega)y, \quad v_{\rm ext} = (\gamma - \Omega)x \tag{2}$$

can destabilize a vortex of sufficiently great height-to-width aspect ratio. Here γ is the strain rate, and Ω is the rotation rate of the strain axes, in a reference frame rotating with Ω. This straining flow is the leading-order approximation of the flow induced by distant columnar vortices surrounding a given vortex. DTJ showed, for example, that two columnar vortices exert a strain on each other of this form, and that the joint instability of the two vortices – which results in merger – can be explained by the instability of each vortex in the straining field of the other.

It is plausible, as discussed next, that this instability also underlies the merger of tall ellipsoidal vortices. Here, however, the ellipsoids are not initially in equilibrium, nor are they columnar. Yet, tall vortices appear locally columnar, especially near their mid-sections where $|z| \ll h$, and the unsteadiness is most significant only far from this region. Moreover, one can regard the initial ellipsoidal state as a perturbed form of a nearby equilibrium state. And lastly, during the early period of the flow evolution, the vortex cross-sections remain very nearly circular while shearing vertically. This is the trademark of the tall-column instability discussed by DTJ (see also Appendix B for further details).

For two columnar vortices of equal radius R and equal PV Q, the strain generated by one vortex in the vicinity of the other is given by $\gamma = \frac{1}{2}Q(R/d)^2$, where d is the vortex separation and here $d \gg R$ is assumed. Meanwhile, the two vortices rotate about each other at the rate $\Omega = 2\gamma$. The analysis in Appendix B shows that, when the dimensionless strain $\hat{\gamma} = \gamma/Q \ll 1$, i.e. when $d \gg R$, a vortex is unstable for a range of dimensionless axial wavenumbers $\hat{k} = kR$ closely satisfying

$$(g(\hat{k}) - \hat{\Omega})^2 < \hat{\gamma}^2$$

where

$$g(\hat{k}) = \tfrac{1}{2} - I_1(\hat{k})K_1(\hat{k}) \approx \tfrac{1}{4}\hat{k}^2[0.36593152\ldots - \log\hat{k}] \tag{3}$$

for $\hat{k} \ll 1$. For $\Omega = 2\gamma$, there is both a long-wave and a 'short'-wave cutoff (still with $\hat{k} \ll 1$). The short-wave cutoff implies that vortices which are too short are stable,

https://doi.org/10.1017/S0022112001007364 Published online by Cambridge University Press

because the wavenumbers available to a columnar vortex in a domain of height H are given by $k = n\pi/H$, $n = 1, 2, 3, \ldots$. Therefore, the above expression, ignoring the $\log \hat{k}$ correction, implies that $H/R \gtrsim \hat{\gamma}^{-1/2}$ for instability. But for two equal columnar vortices, $\hat{\gamma} = \frac{1}{2}(R/d)^2$, so we are left with the simple relation $H/R \gtrsim d/R$ or $H \gtrsim d$ for instability, i.e. for the merger of two vortex columns.

This simple relation is consistent with the critical merger distance found for ellipsoidal vortices in figure 9, if we replace H by h, the half-height of each vortex. One can show that the strain induced by each vortex initially at the centre of the other satisfies

$$\gamma = \frac{R^2}{2d^2} F(a)$$

where

$$F = \frac{\sqrt{1+a^2}}{a} - \frac{1}{a^2} \log(\sqrt{1+a^2} + a) \tag{4}$$

and $a = h/d$. In the two-dimensional limit, $a \to \infty$, we have $F \to 1$, while in the opposite limit for a shallow lens, $a \to 0$, we have $F \to \frac{2}{3}a$. On the other hand, the rotation rate (computed from the angular velocity at the vortex centres) satisfies

$$\Omega = \frac{R^2}{d^2} F(a) \tag{5}$$

with the same functional dependence on a. Thus, just as for vortex columns, here we have $\Omega = 2\gamma$. The effect of $a = O(1)$ is only to reduce the strain rate somewhat from that applicable to columnar vortices (e.g. $F(1) = 0.53284\ldots$). Hence, the strain field near the vortex mid-sections is of the same form and magnitude as for columnar vortices. Finally, to carry over the results of the columnar vortex stability analysis, we need to estimate the 'disturbance' axial wavenumber, but one is naturally provided by the axial variation of the ellipsoid, i.e. $k = O(1/h)$. By analogy with the columnar case, we then have $h \gtrsim d$ as the condition for vortex merger.

It is difficult to be much more quantitative, since several logarithmic factors and $O(1)$ constants have been omitted. Moreover, the initial flow is not in equilibrium. Efforts were made to use the ideas of slender vortex theory (cf. Krause & Gersten 1998) applicable when the vortex cross-section is narrow compared with characteristic axial scales, but none of the standard approximations were sufficiently accurate to reproduce the simulated results. For example, using the leading-order local induction approximation misses out an important non-local contribution coming from the rest of the vortex. Using direct integrations along vortex line elements with a modified, non-singular Green function that includes the local vortex cross-section $\bar{r}(z)$ (i.e. $-1/4\pi\sqrt{|\boldsymbol{x} - \boldsymbol{x}'|^2 + \bar{r}^2(z')}$) did not give sufficiently accurate results either. It appears that the displacement of the core depends sensitively on an accurate representation of the core, and even if it is of nearly circular shape, one must be careful to carry out the integration accurately over the cross-section. This gives rise to a proliferation of elliptic integrals, and the resulting model would hardly simplify the direct simulation method used here.

5. Conclusions

This paper has re-examined the merger of symmetric vortices in a three-dimensional quasi-geostrophic fluid. New numerical results have extended the range of vortex height-to-width aspect ratios previously investigated and have shown that merger

https://doi.org/10.1017/S0022112001007364 Published online by Cambridge University Press

continues at large aspect ratios. Theoretical results on the instability of tall vortex columns support the trend found in the numerical results. Merger occurs for ellipsoidal vortices whose height h (scaled on f/N) roughly exceeds their initial separation distance d. There appears to be no two-dimensional limit as $h/d \to \infty$. Vortices of any height, in an unbounded domain, merge in a three-dimensional fashion if $d \lesssim h$.

This conclusion was not expected by HX who considered the same problem. Nor did they expect asymmetric interactions to occur. The present results indicate that such asymmetric interactions are in fact commonplace. Their existence reveals a surprising richness to vortex interactions even when the initial conditions are highly idealized. This presents a real challenge for quantifying 'typical' vortex interactions in rotating, stratified flows. The study here of symmetric vortices only scratches the surface of a much larger problem, namely the interaction of unequal-sized vortices at different vertical levels. In turbulence, it is rare that two vortices of comparable volume, shape, and mean height are found on the brink of merger. It is therefore important to analyse simulations of turbulence for the generic forms of vortex interactions. Such an analysis would help to focus research on the most relevant forms of interaction.

Appendix A. The unbounded QG contour surgery algorithm

This Appendix discusses the numerical algorithm used for most of the simulations reported. The algorithm is a straightforward extension of the 'contour surgery' algorithm developed for three-dimensional QG flow by Dritschel & Saravanan (1994). Only the essential differences are discussed here.

The starting point is (1b); the inversion of Laplace's operator in three dimensions is affected by the Green function $G(r) = -1/(4\pi r)$, where $r = |\boldsymbol{x}' - \boldsymbol{x}|$ is the (three-dimensional) distance between the 'source' point $\boldsymbol{x}'$ and the 'target' point $\boldsymbol{x}$. Now consider a piecewise-uniform distribution of potential vorticity q. For simplicity, let there be just one contour $\mathscr{C}$ at each height z, into which q jumps by $\Delta q(z)$. Since (1b) is linear in ψ and q, the general case of any number of contours can be obtained by linear superposition. In Dritschel (1989), it is shown that when the Green function depends only on coordinate differences, as here, the velocity field can be expressed in terms of (right-handed) contour integrals over the Green function. Explicitly, we have

$$\boldsymbol{u}(\boldsymbol{x}) = (u, v) = -\int \mathrm{d}z' \Delta q(z') \oint_{\mathscr{C}(z')} G(r)(\mathrm{d}x', \mathrm{d}y') \tag{A 1}$$

(Stokes' theorem is used to convert the area integral to a contour integral).

In the numerical algorithm, the height is discretized into n layers of equal thickness Δz. Only the finite height range spanning the vortices needs to be discretized. Over each layer, Δq and the contour position (x', y') are assumed to be independent of height. Then, the integral over each layer can be performed analytically. It is evaluated at the middle of each layer $\bar{z}_j$ to give (an approximation to) the velocity of any contour in that layer (with an error of $O(\Delta z^2)$). The final expression for the velocity at a point (x, y) in layer j is

$$\boldsymbol{u}_j(x, y) = \frac{1}{4\pi} \sum_{k=1}^{n} \Delta q_k \oint_{\mathscr{C}_k} [\lambda_{jk}^{+} - \lambda_{jk}^{-}](\mathrm{d}x_k', \mathrm{d}y_k') \tag{A 2}$$

where $\lambda_{jk}^{\pm} \equiv \log[(\rho^2 + (|z_{jk}| \pm \frac{1}{2}\Delta z)^2)^{1/2} + |z_{jk}| \pm \frac{1}{2}\Delta z]$, $\rho^2 \equiv (x - x_k')^2 + (y - y_k')^2$, and $z_{jk} = \bar{z}_j - \bar{z}_k$ is the height difference between layers j and k. Now, all of the $\lambda_{jk}^{\pm}$ are non-singular as the two-dimensional distance $\rho \to 0$ except for λ_{jj}^{-}. The latter contains

https://doi.org/10.1017/S0022112001007364 Published online by Cambridge University Press

a logarithmic singularity, the two-dimensional Green function in fact, and it is useful to deal with it separately, using $\lambda^+_{jj} - \lambda^-_{jj} = 2\lambda^+_{jj} - 2\log\rho$. The integral over $\log\rho$ is done explicitly, as described in Dritschel (1989), to avoid numerical instability. The remaining non-singular functions $\lambda^{\pm}_{jk}$ are integrated by parts to give simpler functions (which can be evaluated much more rapidly than logarithms); using now $\boldsymbol{x} \equiv (x, y)$, this gives for $j \neq k$

$$\oint_{\mathscr{C}_k} [\lambda^+_{jk} - \lambda^-_{jk}]\,\mathrm{d}\boldsymbol{x}'_k = \oint_{\mathscr{C}_k} (\boldsymbol{x}'_k - \boldsymbol{x}_j) \left[\frac{1}{(c^+_{jk}\rho^2 + 1)^{1/2}} - \frac{1}{(c^-_{jk}\rho^2 + 1)^{1/2}} \right] \frac{(\boldsymbol{x}'_k - \boldsymbol{x}_j)\cdot \mathrm{d}\boldsymbol{x}'_k}{\rho^2} \quad \text{(A 3)}$$

where $c^{\pm}_{jk} \equiv (|z_{jk}| \pm \frac{1}{2}\Delta z)^{-2}$, and for $j = k$

$$\oint_{\mathscr{C}_j} 2\lambda^+_{jj}\,\mathrm{d}\boldsymbol{x}'_j = \oint_{\mathscr{C}_j} (\boldsymbol{x}'_j - \boldsymbol{x}_j) \left[\frac{\Delta z}{(\rho^2 + \frac{1}{4}\Delta z^2)^{1/2}} - 2 \right] \frac{(\boldsymbol{x}'_j - \boldsymbol{x}_j)\cdot \mathrm{d}\boldsymbol{x}'_j}{\rho^2}. \quad \text{(A 4)}$$

These integrals are carried out using two-point Gaussian quadrature along the piecewise cubic curves connecting adjacent nodes. Details may be found in Dritschel (1989).

Appendix B. The tall-column instability in the weak strain limit

This Appendix indicates how to obtain an accurate estimate of the stability of a columnar vortex when the dimensionless external strain $\gamma/Q \equiv \hat{\gamma} \ll 1$. The analysis follows that of DTJ. We consider here only flows in which the background rotation Ω is comparable to or less than γ. These flows typify virtually all forms of vortex interactions. For example, two equal vortices exert a straining flow on each other that has $\Omega = 2\gamma$, while two opposite vortices have $\Omega = 0$. Here, we define $\beta = \Omega/\gamma$ and consider $\beta = O(1)$.

Without loss of generality, we take $Q = 1$, allowing us to drop the hats from γ and Ω. Then, when $\gamma \ll 1$, the steady basic state is an elliptical column very close to a circular shape; its aspect ratio satisfies $\lambda = 1 - 4\gamma + O(\gamma^2)$. This is used to simplify the general stability equation given at the top of page 134 in DTJ, namely

$$\frac{\partial \eta}{\partial t} + \Omega_e \frac{\partial \eta}{\partial \theta} = \frac{q}{2\pi} \frac{\partial}{\partial \theta} \int_0^{2\pi} \eta(\theta', t) K_0(k|\boldsymbol{x}_e(\theta) - \boldsymbol{x}_e(\theta')|\,\mathrm{d}\theta' \quad \text{(B 1)}$$

where $\mathrm{Re}[\eta(\theta, t)\mathrm{e}^{\mathrm{i}kz}]$ is the normal displacement of the contour from an elliptical shape, θ is the elliptical angular coordinate, k is the axial wavenumber, $\boldsymbol{x}_e(\theta) = (\lambda^{1/2}\cos\theta, \lambda^{-1/2}\sin\theta)$ is the basic-state vortex boundary position, and Ω_e is the value of $\mathrm{d}\theta/\mathrm{d}t$ for the undisturbed flow. For $\lambda = 1 - 4\gamma + O(\gamma^2)$, we have

$$\Omega_e = \tfrac{1}{2} - \beta\gamma + O(\gamma^2).$$

The results of DTJ indicate that the range of unstable wavenumbers shrinks towards $k = 0$ as $\gamma \to 0$, so we assume that $k^2 = O(\gamma)$ in (B 1). Now, in this long-wave limit, it is expected that the different azimuthal modes decouple (since they do for $k = 0$), so we try a disturbance of the form

$$\eta(\theta, t) = [\hat{\eta}_+ \mathrm{e}^{\mathrm{i}m\theta} + \hat{\eta}_- \mathrm{e}^{-\mathrm{i}m\theta}]\mathrm{e}^{-\mathrm{i}\sigma t}$$

where the imaginary part of σ is the growth rate (a general disturbance consists of a sum over the azimuthal wavenumber m). Moreover, for the tall-column instability,

https://doi.org/10.1017/S0022112001007364 Published online by Cambridge University Press

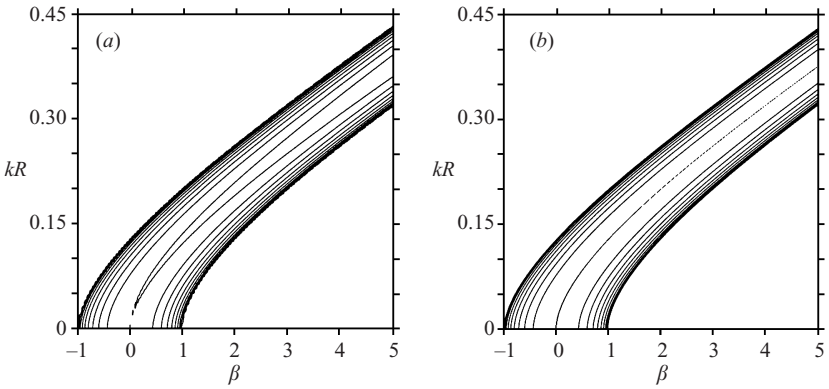


FIGURE 12. Growth rate of perturbations to an elliptical column scaled on the strain rate γ as a function of $\beta = \Omega/\gamma$ and vertical wavenumber k. Here, $\gamma = 0.01$. The exact result, obtained via the analysis described in DTJ, is shown in (a), while the approximate result, from (B 2), is shown in (b). The contour interval is 0.1.

we know from DTJ that it is dominated by $m = 1$, so we consider only this value of m in what follows.

The integral over the K_0 Bessel function in (B 1) can be performed analytically after expanding its argument to first order in γ. That is, using

$$|\boldsymbol{x}_e(\theta) - \boldsymbol{x}_e(\theta')| \approx [2(1-\cos\alpha)]^{1/2}[1 + 2\gamma\cos(\alpha + 2\theta)]$$

with $\alpha \equiv \theta' - \theta$, we have

$$K_0(k|\boldsymbol{x}_e(\theta) - \boldsymbol{x}_e(\theta')| \approx K_0(k[2(1-\cos\alpha)]^{1/2}) - 2\gamma\cos(\alpha + 2\theta).$$

Now, any function of the form $e^{im\alpha}$ multiplied by either term can be integrated directly (see Waugh & Dritschel 1991 for integrals involving this K_0 function); the result is

$$\begin{aligned}(\Omega_e - \sigma)\hat{\eta}_+ &= \chi(k)\hat{\eta}_+ + \gamma\hat{\eta}_-,\\ (-\Omega_e - \sigma)\hat{\eta}_- &= -\chi(k)\hat{\eta}_- - \gamma\hat{\eta}_+,\end{aligned} \tag{B 2}$$

where $\chi(k) \equiv I_1(k)K_1(k)$. We have here ignored any term not involving $e^{\pm i\theta}$. Solvability then gives

$$\sigma = \pm[(g(k) - \beta\gamma)^2 - \gamma^2]^{1/2} \tag{B 3}$$

where $g(k) = \frac{1}{2} - I_1(k)K_1(k)$. Since $g(k) = O(k^2\log k)$, instability only occurs when $k = O(\gamma^{1/2})$, approximately. To see how this compares with the full analysis presented in DTJ for arbitrary k, figure 12 shows $\mathrm{Im}[\sigma]/\gamma$ for the asymptotic result above in (b), and for the full analysis in (a), for the value $\gamma = 0.01$. Apart from a slight difference in the maximum growth rate, the results are otherwise remarkably close. This demonstrates that the tall-column instability occurs because two counter-propagating helical modes, $e^{\pm i\theta + ikz}$, become phase-locked by the background strain.

REFERENCES

CAILLOL, P., LEGRAS, B. & DRITSCHEL, D. G. 2001 Erosion of a distributed two-dimensional vortex in a strain flow. *J. Fluid Mech.* **44**, 369–398.

CHARNEY, J. G. 1971 Geostrophic turbulence. *J. Atmos. Sci.* **28**, 1087–1095.

CHRISTIANSEN, J. P. & ZABUSKY, N. J. 1973 Instability, coalescence and fission of finite-area vortex structures. *J. Fluid Mech.* **61**, 219–243.

DRITSCHEL, D. G. 1989 Contour dynamics and contour surgery: numerical algorithms for extended,

https://doi.org/10.1017/S0022112001007364 Published online by Cambridge University Press

high-resolution modelling of vortex dynamics in two-dimensional, inviscid, incompressible flows. *Comput. Phys. Rep.* **10**, 77–146.

Dritschel, D. G. 1995 A general theory for two-dimensional vortex interactions. *J. Fluid Mech.* **293**, 269–303.

Dritschel, D. G. & Saravanan, R. 1994 Three-dimensional quasi-geostrophic contour dynamics, with an application to stratospheric vortex dynamics. *Q. J. R. Met. Soc.* **120**, 1267–1297.

Dritschel, D. G. & Ambaum, M. H. P. 1997 A contour-advective semi-Lagrangian algorithm for the simulation of fine-scale conservative fields. *Q. J. R. Met. Soc.* **123**, 1097–1130.

Dritschel, D. G. & Macaskill, C. 2000 The role of boundary conditions in the simulation of rotating, stratified turbulence. *Geophys. Astrophys. Fluid Dyn.* **92**, 233–253.

Dritschel, D. G., Polvani, L. M. & Mohebalhojeh, A. R. 1999 The contour-advective semi-Lagrangian algorithm for the shallow-water equations. *Mon. Wea. Rev.* **127**, 1151–1165.

Dritschel, D. G. & de la Torre Juárez, M. 1996 The instability and breakdown of tall columnar vortices in a quasi-geostrophic fluid. *J. Fluid Mech.* **328**, 129–160 (referred to herein as DTJ).

Dritschel, D. G., de la Torre Juárez, M. & Ambaum, M. H. P. 1999 The three-dimensional vortical nature of atmospheric and oceanic turbulent flows. *Phys. Fluids* **11**, 1512–1520.

Dritschel, D. G. & Waugh, D. W. 1992 Quantification of the inelastic interaction of two asymmetric vortices in two-dimensional vortex dynamics. *Phys. Fluids* A **4**, 1737–1744.

Dritschel, D. G. & Zabusky, N. J. 1996 On the nature of vortex interactions and models in unforced nearly-inviscid two-dimensional turbulence. *Phys. Fluids* **8**, 1252–1256.

von Hardenburg, J., McWilliams, J. C., Provenzale, A., Shchepetkin, A. & Weiss, J. 2000 Vortex merging in quasi-geostrophic flows. *J. Fluid Mech.* **412**, 331–353 (referred to herein as HX).

Hoskins, B. J., McIntyre, M. E. & Robertson, A. W. 1985 On the use and significance of isentropic potential-vorticity maps. *Q. J. R. Met. Soc.* **111**, 877–946.

Krause, E. & Gersten, K. (Eds.) 1998 *Dynamics of Slender Vortices* (*Proc. IUTAM Symp., Aachen, 31 August–September 1997*), pp. 235–244. Kluwer.

McWilliams, J. C. 1990 The vortices of geostrophic turbulence. *J. Fluid Mech.* **219**, 387–404.

McWilliams, J. C., Weiss, J. B. & Yavneh, I. 1994 Anisotropy and coherent vortex structures in planetary turbulence. *Science* **264**, 410–413.

Meacham S. P., Pankratov, K. K., Shchepetkin, A. F. & Zhmur, V. V. 1994 The interaction of ellipsoidal vortices with background shear flows in a stratified fluid. *Dyn. Atmos. Oceans* **21**, 167–212.

Saffman, P. G. 1992 *Vortex Dynamics*. Cambridge University Press.

Stegner, A. & Zeitlin, V. 1995 What can asymptotic expansions tell us about large-scale quasi-geostrophic anticyclonic vortices? *Nonlinear Processes Geophys.* **2**, 186.

Verron, J., Hopfinger, E. J. & McWilliams, J. C. 1990 Sensitivity to initial conditions in the merging of two-layer baroclinic vortices. *Phys. Fluids* A **2**, 886–889.

Waugh, D. W. 1992 The efficiency of symmetric vortex merger. *Phys. Fluids* A **4**, 1745–1758.

Waugh, D. W. & Dritschel, D. G. 1991 The stability of filamentary vorticity in two-dimensional geophysical vortex-dynamics models. *J. Fluid Mech.* **231**, 575–598.

Yao, H. B., Dritschel, D. G. & Zabusky, N. J. 1995 High-gradient phenomena in 2D vortex interactions. *Phys. Fluids* **7**, 539–548.

https://doi.org/10.1017/S0022112001007364 Published online by Cambridge University Press